Journal of Engineering Physics and Thermophysics, Vol. 79, No. 6, 2006

EXPERIMENTAL STUDY OF THE FRICTION STRESS AND TRUE GAS CONTENT IN UPWARD BUBBLY FLOW IN A VERTICAL TUBE

O. N. Kashinckii, L. S. Timkin, R. S. Gorelik, and P. D. Lobanov

UDC 532.529.5

An experimental study of the laminar, transient, and turbulent conditions of the flow of monodispersed gas-liquid mixtures with one- and two-millimeter bubbles has been made. Tube-parameter-averaged data on the development of friction stress on the wall and its pulsations have been obtained. The asymmetry parameter characterizing the nonuniformity of the friction stress distribution along the tube perimeter has been introduced. Flow conditions with a strong asymmetry have been revealed. The true gas content has been calculated by the Zuber–Hench formula [1]. For flow conditions with wall peaks of the gas content, the calculation data are in good agreement with the experimental data.

The upward bubbly flow is used in various fields of science and engineering, but there are still problems of determining the physical mechanisms governing the flow and of calculating the basic characteristics of the flow. A large number of parameters such as the Reynolds number of the flow, the Reynolds number for the bubble, the Morton and Etvish numbers, the scale parameters, etc. make analysis of such a flow an essentially multidimensional problem. Even under turbulent, most extensively studied flow conditions [2–5], because of the interaction between the bubble-induced pseudoturbulence and the natural turbulence of the liquid, the influence of Reynolds numbers on the average and pulsation characteristics of the flow is not always clear. To simulate flows of a bubbly mixture, one often uses additivity of the pseudoturbulence and natural turbulence of the liquid [4]. However, in experiments also regimes with a strongly nonlinear character of interaction between these components are not infrequent. The pseudoturbulence has been investigated many times under laminar conditions of the bubbly mixture flow at laminar Reynolds flow numbers [6–10] when only pulsations induced by the dispersed phase are present. Even simple listing of individual sources of pseudoturbulence [11] gives an idea about the complexity of the laws of its development and interaction with the natural turbulence of the liquid:

a) perturbation of the liquid velocity field due to the presence of dispersed-phase particles;

b) pulsations generated in traces and on the surface of particles;

c) hydrodynamic interaction between the natural turbulence of the liquid and the surface of particles leading to an increase or suppression of single-phase pulsations of the liquid;

d) interaction of particles through the liquid phase leading to a change in their paths, and the generation of dispersed phase velocity fluctuations and additional pulsations of the liquid phase velocity because of the added mass of bubbles.

The upward bubbly flow has asymmetry noted at low velocities of the liquid [12, 13]. As a result, the friction stress measured at one point on the wall may differ considerably from its average over the tube perimeter. In the absence of proper spatial averaging the flow asymmetry limits the accuracy of experiments and comparison with the calculation. The question of asymmetry of bubbly flows has been insufficiently covered in the literature.

One major parameter of the flow is the true volume gas content. In the literature there exist many different correlations for its calculation. In the work of Zuber and Findley [14] it was shown that the relation between the true gas content and the flow parameters depends on the flow conditions of the gas-liquid mixture. The authors' approach

Institute of Thermal Physics, Siberian Branch of the Russian Academy of Sciences, 1 Akad. Lavrent'ev Ave., Novosibirsk, 630090, Russia; email: timkin@itp.nsc.ru. Translated from Inzhenerno-Fizicheskii Zhurnal, Vol. 79, No. 6, pp. 68–80, November–December, 2006. Original article submitted February 16, 2005.

1062-0125/06/7906-1117 ©2006 Springer Science+Business Media, Inc.

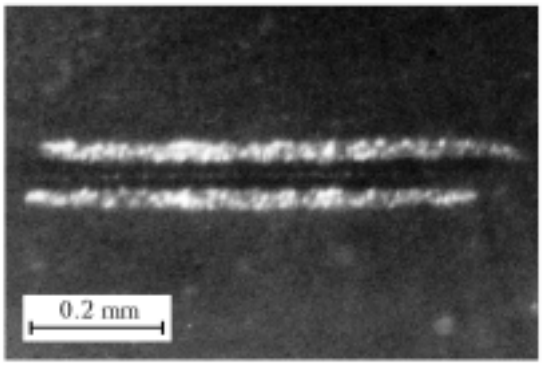

Fig. 1. Dual electrochemical pickup pasted in the wall of the measuring section.

made it possible to classify the flow conditions. Now the interest in this work has been renewed due to the simplicity and graphicness of the proposed model [15–17].

The aim of the present paper is to expand the notion about the behavior of the upward bubbly flow under laminar, transient, and turbulent flow conditions. We have made an experimental study of the friction stress on the wall and its pulsations for two sizes of bubbles from laminar-laminar flow conditions of the mixture (laminar as to the Reynolds number of the flow and laminar as to the Reynolds number of bubbles) to turbulent-turbulent flow conditions. The paper presents the flow conditions with both pure pseudoturbulent pulsations and simultaneous presence of natural turbulence of the liquid and pseudoturbulence. Particular consideration is given to the flow asymmetry and the correlation between the true volume gas content and the expended one.

Experimental Facility. A vertical tube from stainless steel of internal diameter 14.8 mm and height 6.5 m is equipped with a bottom tank with an immersion pump, a thermostabilization system, a top tank with a gas separator, and systems for controlling and measuring the gas and liquid flow rates. At the inlet into the tube a gas-liquid mixer with changeable bubble generators which permitted obtaining monodispersed bubbly mixtures was placed. The bubble generators were positioned axisymmetrically in the mixer. Bubbles were formed in the mixer under conditions close to the conditions of a large volume, then they were picked up by the liquid flow which was smoothly compressed and entered the tube. In the generator, for one-millimeter bubbles several changeable rings with a different number of inlet holes were used. Therefore, upon their change there was a small stepwise change in the diameter of bubbles, which gave rise to an insignificant error in measurements. The working section with a measuring unit was located at a distance of 5.25 m from the mixer. The facility is described in more detail in [18]. As a working fluid, we used a standard electrochemical solution [19] into which glycerol was added for increasing viscosity.

Measurement Procedure. To register the friction stress on the wall, the electrodiffusion method was used [19]. Eight dual pickups were uniformly located in the measuring unit along the tube perimeter and were used to determine the amplitudes and signs of local friction stresses on the wall. Each pickup consisted of two platinum electrodes of size 700×40 μm separated by a thin insulating layer. The photograph of the pickup pasted in the tube wall (magnification of 40 diameters) is given in Fig. 1. Upon amplification in the primary apparatus the pickup currents were recorded by means of a Lcard 16-digit L-1620 multichannel analog-to-digital converter.

Calibration of the pickups was carried out in the working tube just before measurements with the use of the relative method [19]. The friction stress on the wall was calculated by the Hagen–Poiseuille and Blasius relations. In so doing, both the first and second electrodes of the pickups were connected to individual amplifiers. In the upward flow, the first, in the flow, electrodes were first calculated. Then the measuring unit was turned over and the procedure was repeated with the second electrodes. The electrode current was converted by the calibration factors to the friction stress, and then the effective current values were determined as the cube root of the friction stress. Under operation of the pickups in a single-phase flow the current of the second electrode located in the diffusion trail from the first one decreases by 15–30%, and upon reversal of the flow — vice versa. To determine the sign of the friction stress, the effective current values were used. As a criterion for this, we chose a 3.3% excess of the effective current of one electrode over the other. This procedure is a digital analog of equalization of currents of both electrodes for a dual friction pickup performed earlier in analog form [19].

TABLE 1. Characteristics of the Process Solutions and Parameters of Bubbles

Solution number	ρ_{liq}, kg/m^3	$\nu \cdot 10^6$, m^2/sec	d_b = 1.2 mm		d_b = 2.2 mm	
			V_∞, m/sec	Re_b	V_∞, m/sec	Re_b
1	1170	9.8	0.049	6	0.102	23
2	1124	3.5	0.093	32	0.160	101
3	1031	1.06	0.131	148	0.220	460

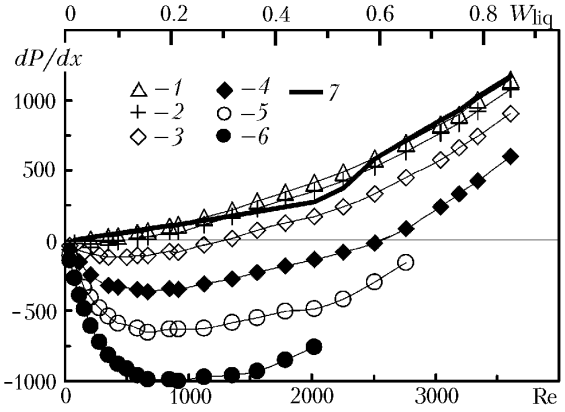

Fig. 2. Pressure drop for transient flow conditions (d_b = 2.2 mm): 1) β = 0.0043; 2) 0.017; 3) 0.043; 4) 0.0865; 5) 0.130, 6) 0.174; 7) experimental single-phase drop. dP/dx, N/m^2; W_{liq}, m/sec.

For each pickup, alternating friction was determined and a data array on friction (10,000–16,000 readings per pickup with an interval between readings from 0.1 to 5 msec) was formed depending on the flow rate. Average and pulsation characteristics of the friction stress were finally calculated in the program regime on a Pentium II computer.

In the single-phase flow, the difference between the measured and calculated friction values for each pickup did not exceed 5% except for the small reduced velocities of the liquid ($W_{liq} \le 0.05$ m/sec). Here the analog noise of the facility became significant and the error reached 7%. As the alternating friction got over zero, the relative measurement error increased, but the absolute error was small, since the friction values are low and the transition process is fairly fast. Calibration of the pickups was carried out in a maximally wide range of flow rates with approximation to zero values. Therefore, the friction measurement error in the two-phase flow is within $\pm$10%.

In using three process solutions with different viscosities (see Table 1), the following flow conditions were obtained: laminar (Re = 20–1000), transient (Re = 60–3700), and turbulent ones (Re = 200–14,000). Data series were taken at a constant volume gas content $\beta = W_g/(W_g + W_{liq})$, and the reduced gas velocity W_g was taken at atmospheric pressure. With further data processing the volume gas content was recalculated with allowance for the hydrostatic weight of the bubbly mixture column over the working part which was estimated by the experimentally measured pressure drop. Thus, the accuracy of maintaining the volume gas content turned out to be of the order of 1.5% (mainly due to the change in the weight of the mixture column at different expenditure parameters). In the work, monodispersive gas-liquid mixtures with two mean bubble diameters of 1.2 and 2.2 mm were used (see Table 1). The rms spread of bubble diameters was within 15%. For the intermediate-viscosity solution the emergence rate of bubbles was determined by the experimental correlation given in [18], and for the other solutions — by the known dependences for solid spheres [20].

Pressure Drop. To measure the pressure drop, we used a U-shaped manometer with a reading accuracy of the order of 2–3 mm of water. The drop was composed from the drop resulting from the two-phase friction on the wall and the drop due to the decrease in the working mixture viscosity at the cost of bubbles (the hydrostatic weight of the pure liquid column was substracted from it). The experimental data on the pressure drop per 1 m of the tube for two-millimeter bubbles and the process solution with viscosity $\nu = 3.5 \cdot 10^{-6}$ m^2/sec are presented in Fig. 2. For the single-phase flow it coincides with the values obtained from the Hagen–Poiseuille and Blasius laws for laminar and turbulent flow conditions respectively (semiboldface curve in Fig. 2). The laminar–turbulent transition in the single-phase liquid

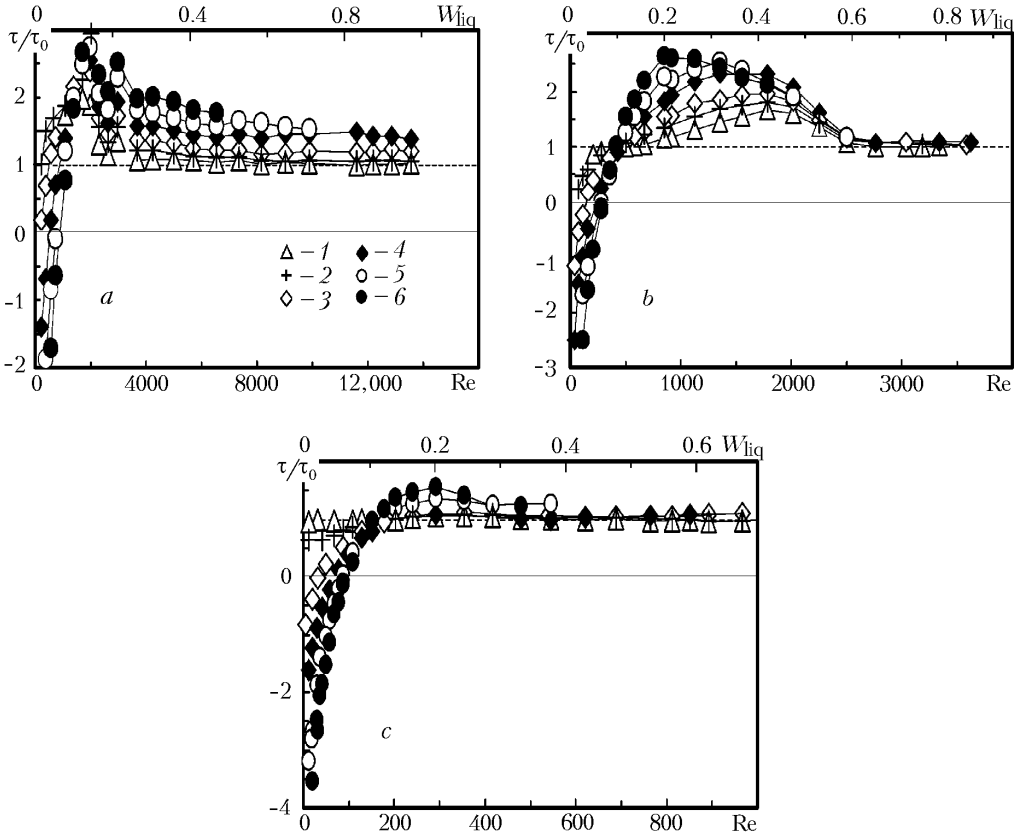

Fig. 3. Ratio of the tube-perimeter-average two-phase friction stress on the wall to the single-phase one versus Re (d_b = 2.2 mm): a) $\nu = 1.06 \cdot 10^{-6}$ m^2/sec; b) $3.5 \cdot 10^{-6}$; c) $9.8 \cdot 10^{-6}$. Designations 1–6 same as in Fig. 2. W_{liq}, m/sec.

occurs ar Reynolds flow numbers Re = 1800–2020. In the majority of investigated regimes, the influence of bubbles leads to a decrease in the pressure drop to values below the single-phase ones due to the decrease in the mixture density and the appearance of negative friction stresses caused by the reverse wall flows. At a fixed Reynolds number the influence of bubbles increases with increasing gas content of the flow. At large gas contents a pronounced minimum of the pressure drop appears. At lower Reynolds numbers reverse wall flows arise, and the bubbles go from the wall to the near-axis part of the tube.

In the transient regime at Reynolds numbers Re = 1500–2500 and volume gas contents $\beta < 0.043$ the influence of bubbles leads to a larger pressure drop than in the single-phase flow (Fig. 2). At a fixed Reynolds number a nonmonotonic change in the pressure drop with increasing gas content associated with the strong interaction of bubbles with the wall and the sharp increase in the friction stress on it is observed here. As a result, the friction contribution exceeds the decrease in the pressure drop due to the change in the mixture density. The nonmonotonic character for one-millimeter bubbles is more pronounced than for two-millimeter ones.

Tube-Perimeter-Average Friction Stress on the Wall. One of the main tasks of this work was to register reverse flows on the wall arising at small Reynolds numbers [21]. The negative friction observed in the experiment makes it impossible to represent data in the form of the drag coefficient. Therefore, here the data are given as the ratio of the two-phase friction stress on the wall to the single-phase one τ/τ_0 at one and the same Reynolds number. Figure 3 shows the dependence of this ratio on the Reynolds number (dashed line represents the value of $\tau/\tau_0 = 1$) for two-millimeter bubbles at different volume gas contents of the mixture under laminar (Fig. 3c), transient (Fig. 3b), and turbulent (Fig. 3a) flow conditions.

The dependences of the ratio of friction values are similar for all the three kinds of flow conditions. The common characteristic features are:

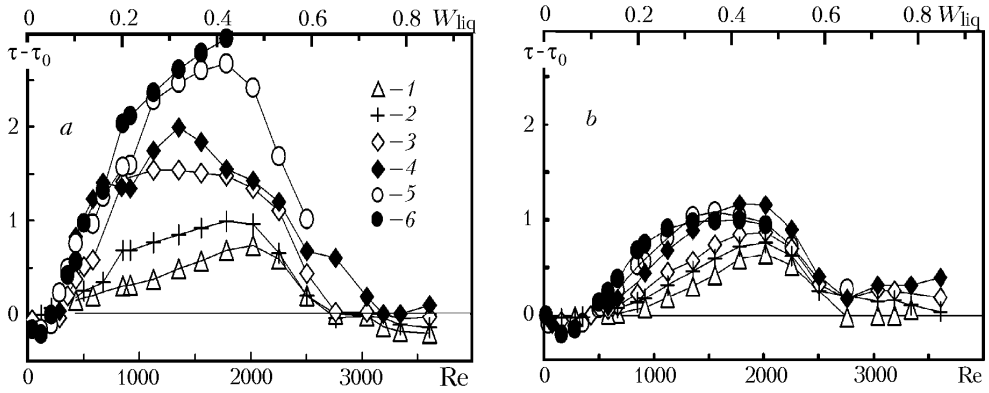

Fig. 4. Perturbation of the friction stress on the wall introduced by bubbles at a solution viscosity $\nu = 3.5 \cdot 10^{-6}$ m^2/sec: a) d_b = 1.2; b) 2.2 mm. Designations 1–6 same as in Fig. 2. τ, N/m^2; W_{liq}, m/sec.

1) the appearance at small Reynolds numbers of wall reverse flows, which leads to large negative values of the friction ratio depending on the volume gas content;

2) the appearance of a maximum of the friction ratio with increasing Reynolds number;

3) a decrease in the influence of bubbles with further increase in the Reynolds number, approach of the two-phase friction to the single-phase one (at large gas contents in this region there is a small excess of the two-phase friction over the single-phase one which is more pronounced under turbulent conditions, which correlates with the growth of friction pulsations under these conditions and is likely to be only due to the influence of friction pulsations).

For one-millimeter bubbles the range of reverse flows shifts towards smaller Reynolds flow numbers, and the maximum friction is larger than for two-millimeter ones, which is due to the closer approach of small bubbles to the wall.

The differences between the dependences of the friction ratio for different regimes are qualitative. Note that the emergence rate for bubbles is inversely proportional to the liquid density; therefore, at low densities the transverse force that presses small bubbles to the tube wall increases to considerably increase the two-phase friction. In a viscous solution the distance from the wall gas content peak to the wall is comparable to the bubble diameter [8], whereas in a low-viscosity solution bubbles practically slide on the wall tube [12]. The maximum value of the friction ratio τ/τ_0 for 2/1-mm bubbles is 1.5/2.1 in a viscous process solution, 2.6/5.9 in an intermediate one, and 3.0/4.5 in a solution close in viscosity to water.

At a lower liquid viscosity reverse flows arise at larger values of Reynolds numbers and a smaller gas constant. For instance, for the three process solutions and 2/1-mm bubbles reverse flows are registered up to Reynolds numbers of 150/108, 670/430, and 3700/2970, respectively. In the most viscous solution at $\beta = 0.017$ reverse flows are absent, and in the solution close in viscosity to water reverse flows are registered even at $\beta = 0.0043$.

Figure 4 presents the data as a difference between two-phase and one-phase friction stresses $\tau - \tau_0$ on the wall for bubbles of the two sizes and a solution with viscosity $\nu = 3.5 \cdot 10^{-6}$ m^2/sec. In general, the dependences for these bubbles are qualitatively similar. At low liquid velocities the region of reverse flows stands out, then the influence of bubbles increases, reaches its maximum, and decreases. One-millimeter bubbles lead to a friction stress on the wall almost twice larger than two-millimeter ones. In the given solution the influence of bubbles on the average friction decreases in the region of the laminar-turbulent transition in the one-phase liquid and can be due to both the specific features of the interaction of bubbles with the tube wall and the influence of the increasing natural turbulence of the liquid. As a result, there is a change in the flow conditions of the mixture which shows up as a change of the law for the true gas content and a change in the Zuber–Findley parameters.

Friction Stress Pulsations. The tube-perimeter-averaged pulsations of the friction stress on the wall for two-millimeter bubbles and the three process solutions are given in Fig. 5. The semibold face line shows the single-phase turbulent pulsations which begin to develop from Re $\approx$ 1800 (Fig. 5a and b). In the low-viscosity solution (Fig. 5a), two-phase pulsations grow as the Reynolds number of the tube both before and after the laminar-turbulent transition, and the bubble Reynolds numbers thereby are essentially turbulent (see Table 1). In the viscous solution (Fig. 5c) pul-

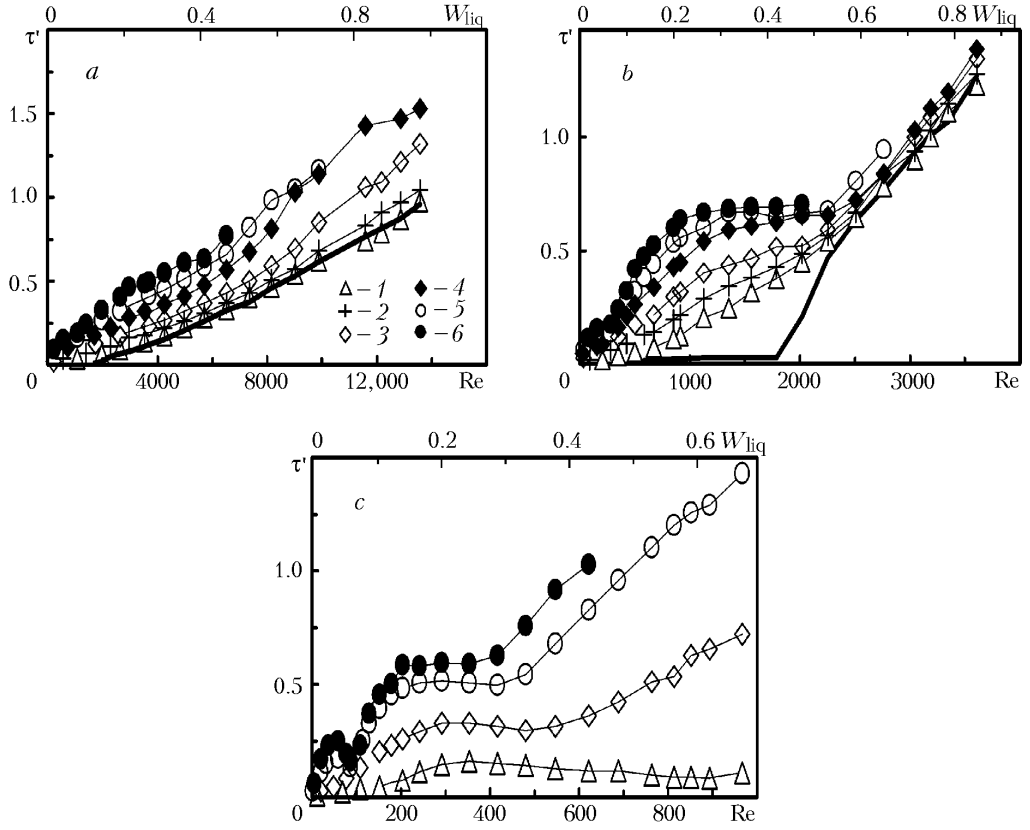

Fig. 5. Tube-perimeter-average pulsations of the friction stress on the wall (d_b = 2.2 mm): a) $\nu = 1.06 \cdot 10^{-6}$; b) $3.5 \cdot 10^{-6}$; c) $9.8 \cdot 10^{-6}$ m^2/sec. Designations 1–6 same as in Fig. 2. τ', N/m^2; W_{liq}, m/sec.

sations are more complex in nature. At small Reynolds numbers (Re ≈ 70) and large gas contents a maximum of pulsations in the reverse flows is noticeable, since the average friction stress thereby is negative. In the range of Re = 200–400, pulsations weakly depend on the Reynolds number and their value is determined by the gas content of the mixture. For conditions with a larger gas content pulsations begin to grow in proportion with Re.

For the Intermediate process solution (Fig. 5b) the development of pulsations combines the properties of the turbulent (growth with the Reynolds number) and laminar flows (the region of constant pulsations and the feature in reverse flows). In a developed single-phase turbulent flow, friction stress pulsations grow proportionally to the friction, as $\tau' = 0.32\tau$ [22]. In the two-phase flow, proportionality of pulsations to the Reynolds number is noted in several regimes: in a viscous solution at large Reynolds numbers and large gas contents; in an intermediate-viscosity solution at Reynolds numbers larger than the value for the transition to turbulence; and in a low-viscosity solution even at Reynolds numbers smaller than the transition value. Since proportionality is an indication of single-phase turbulence, for pseudoturbulent pulsations it is likely to be due to the inner properties of the pseudoturbulence.

At laminar Reynolds numbers, because of the difference in the flow past a bubble (at Reynolds numbers of the bubble larger or smaller than 100) the behavior of pseudoturbulent pulsations changes qualitatively. Pulsations induced by bubbles with $Re_b \geq 100$ grow as the Reynolds number, as in the developed single-phase flow, while in the intermediate-viscosity solution at $Re_b \leq 100$ pulsations at Re > 2000 do not differ widely from single-phase pulsations.

Flow Asymmetry. In [13], it was proposed to use the difference between the integral values of the gas content determined from the left and right halves of the local gas content profile measured on the tube diameter as an asymmetry parameter. This parameter was normalized to the average gas content on the tube cross-section. At low flow rates of the liquid the asymmetry reached maximum values of 15–20%. The asymmetry parameters determined on the basis of different parameters can differ quantitatively, but qualitatively they should register asymmetric flow conditions.

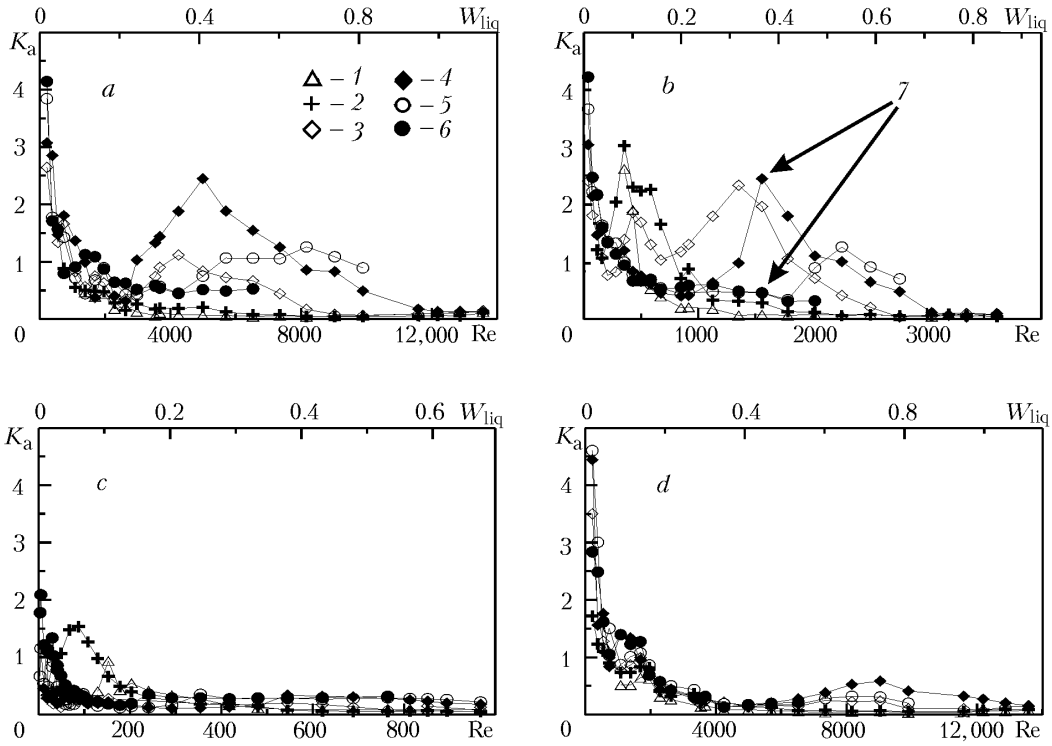

Fig. 6. Asymmetry parameter K_a versus the Reynolds flow number: a) d_b = 1.2 mm, $\nu = 1.06 \cdot 10^{-6}$ m^2/sec; b) 1.2 and $3.5 \cdot 10^{-6}$; c) 1.2 and $9.8 \cdot 10^{-6}$; d) 2.2 and $0.6 \cdot 10^{-6}$. Designations 1–6 same as in Fig. 2. W_{liq}, m/sec.

On the basis of the maximum, on all pickups, friction stress τ_{max}, minimum τ_{min}, and single-phase τ_0 friction stresses, for analysis of the flow it is convenient to introduce the asymmetry parameter

$$K_a = (\tau_{max} - \tau_{min})/\tau_0 . \quad (1)$$

To normalize the parameter, one can use the two-phase friction stress, but such a definition is inapplicable when the two-phase friction vanishes.

The dependences of the asymmetry parameter on the Reynolds number for different regimes are given in Fig. 6. The parameter values are in the range of $0.1 \le K_a \le 4$. This means that in the flow both practically symmetric regimes and strong-asymmetry regimes are realized, which strongly influences measurement data in the absence of proper spatial averaging. In the single-phase flow the parameter values are determined by the accuracy of friction stress measurements and usually equal $K_a \approx 0.1$–0.2. At small Reynolds numbers the asymmetry parameter always has a maximum caused by the specific feature of the liquid running down near the wall under bubbling flow conditions. In this case, the facility noise becomes essential and introduces errors to measurements of small friction stresses. At high Reynolds numbers additional maxima of the asymmetry parameter are registered (at Re = 4000–8000 in Fig. 6a, Re = 500–2200 in Fig. 6b, and Re = 100 in Fig. 6c). The amplitudes of these maxima decrease with increasing viscosity of the process solution. For a fixed solution and different volume gas contents, the position of the maxima is not fixed. The asymmetry parameter for two-millimeter bubbles is smaller, as a rule, than for one-millimeter ones. Detailed analysis has revealed that the additional asymmetry maxima are due to the appearance in the flow of structures of the type of bubble columns. In [23], in a laminar flow the friction perturbation on the wall by a single bubble was analyzed. It was shown that a bubble in a tube of small diameter (14.8 mm) practically always emerges not axisymmetrically. On the part of the tube wall near which it emerges a sharp peak of friction appears, and in the other places the friction decreases. The peak amplitude is 2–5 times larger than the single-phase friction. After the sharp peak (for different flow conditions) a long laminar or turbulent wake is observed. Figure 7 shows two time realizations of friction stress in the form of isolines of constant friction on the wall: Figure 7a corresponds to flow conditions with a

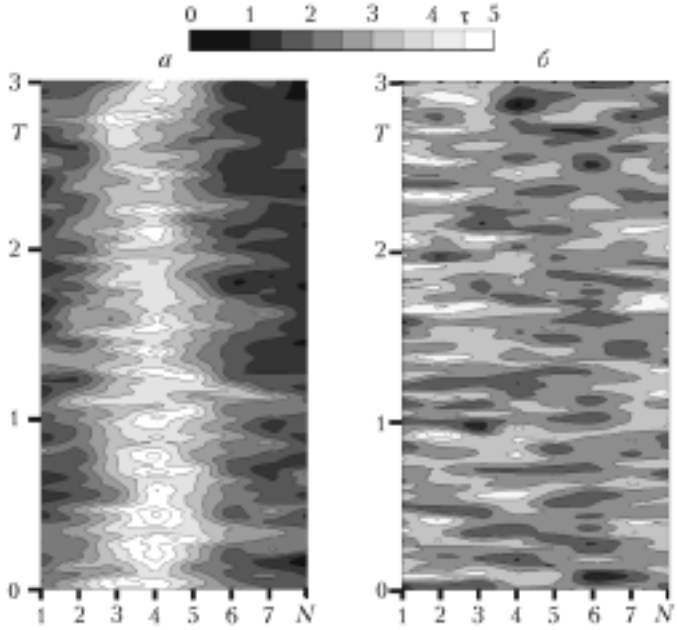

Fig. 7. Friction stress on the wall (d_b = 1.2 mm, $\nu = 3.5 \cdot 10^{-6}$ m^2/sec; Re = 1560, τ_0 = 0.78 N/m^2): a) under asymmetric flow conditions where a bubbly column is formed, β = 0.0865, K_a = 2.9, τ = 2.6 N/m^2; b) at a uniform distribution of bubbles over the tube cross-section, β = 0.130, K_a = 0.54, τ = 3.38 N/m^2. *N*, ordinal number of the friction pickup in the tube cross-section. *T*, sec; τ, N/m^2.

maximum of the asymmetry parameter, and Fig. 7b — to almost symmetric conditions. These conditions are marked by a number 7 in Fig. 6b and only differ by the value of the expenditure gas content. White color shows closed regions corresponding to the maximum perturbation of friction by bubbles. Comparison of the realizations shows that under axisymmetric conditions bubbles come together in a bubbly column near a small part of the tube perimeter (Fig. 7a), and at a small asymmetry parameter they are uniformly distributed along the tube perimeter (Fig. 7b). It has been verified experimentally that the bubbly column can maintain a certain position for a long time, giving a strong asymmetry of the flow. From the analysis of different realizations it has been established that there exist transient regimes where a bubbly column can from time to time spread uniformly along the perimeter and then assemble into a local structure again. This explains the indistinct boundaries of the asymmetric flow conditions in Fig. 6. Such a "visualization" of the friction stress on the wall permits qualitative detection of flow conditions with bubbly columns. For more accurate asymmetry analysis, space-time analysis of the friction realizations is needed.

From the literature cases of the appearance of coherent structures in bubbly flows are known. For instance, [24] presents a review of the works on structures that arise in upward bubbly flows, mainly in airlift systems. A wide variety of arising secondary flows and recirculation cells, especially in three-dimensional facilities, is noted, and, as in Fig. 7a, the flow symmetry is broken. Spectral analysis fails to reveal the characteristic features of the process, and the influence of the liquid flow rate on the observed structures is practically not considered.

True Volume Gas Content. In simulating two-phase bubbly flows, of great importance is the true volume gas content. To estimate it, one often uses the equation of balance of forces

$$dP/dx = 2 \cdot \tau / R - (\rho_{liq} - \rho_g)\, g\alpha\,, \tag{2}$$

where *dP/dx* is the pressure drop per unit length of the tube minus the hydrostatic weight of the pure liquid column; τ is the tube-perimeter-average friction on the wall; and α is the true volume gas content. The results of the experimental estimation of the true volume gas content with viscosity $\nu = 3.5 \cdot 10^{-6}$ m^2/sec and two bubble diameters are presented in Fig. 8. These data were compared to the known Zuber–Hench formula [1] for the drift flow density:

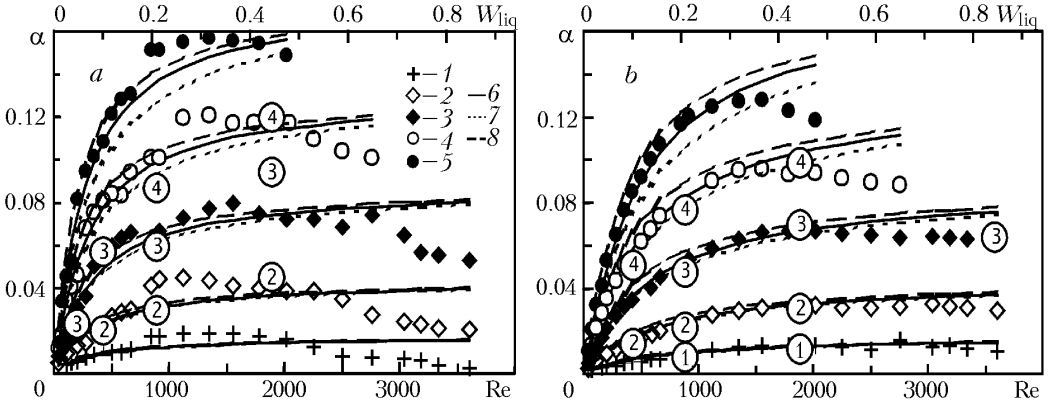

Fig. 8. Comparison of the true volume gas content to the calculation ($\nu = 3.5 \cdot 10^{-6}$ m^2/sec): a) d_b = 1.2 mm; b) 2.2 [1] β = 0.017; 2) 0.043; 3) 0.0865; 4) 0.130; 5) 0.174; 6) calculation according to Zuber and Hench [1] with correlation (4); 7) with correlation (5); 8) with correlation (6)]. W_{liq}, m/sec.

$$j_{21} = W_{liq}(1-\alpha) - W_g\alpha = V_\infty \alpha (1-\alpha)^n = V_\infty \alpha h(\alpha), \tag{3}$$

in which one can single out the drag factor taking into account the slowing-down of a bubble by the surrounding bubbles:

$$h(\alpha) = (1-\alpha)^n, \tag{4}$$

where n = 1.75–2. If we ignore the slowing-down of the bubble by the surrounding bubbles, then $h(\alpha) = 1$. Then for the true gas content the formula widely used in the literature is obtained:

$$\alpha = W_g/(W_g + W_{liq} + V_\infty). \tag{5}$$

Equation (3) was solved for the true volume gas content as a function of the expenditure parameters W_g and W_{liq} with different right sides. In so doing, to calculate α, two approaches were used: numerical solution of the equation for a given value of expenditure parameters and approximate solution consisting of the Taylor expansion of the equation in α powers. In the power expansion the series converges fairly quickly. The volume gas content in the experiments did not exceed β = 0.174 and, therefore, in considering the first three terms of the Taylor expansion (up to α^3) and solving the cubic equation analytically — by the Cardan method, the difference of α from the value in the exact numerical solution did not exceed 2%. The small gas content explains the weak influence of the parameter n on the result, which permitted using one value of n = 2 in all calculations. Figure 8 presents for different data sets the results of the numerical calculations with correlation (4). Note that this is not the only correlation that can be found in the literature. In [17, 18, 25], drag factors with a different dependence on the gas content are given, e.g., in [18]

$$h(\alpha) = (1 - 0.75\alpha^{1/3}). \tag{6}$$

This formula was obtained in local measurements of the sliding velocity and was not used to calculate the integral volume gas content. The power of the dependence 1/3 points to a radical difference of the flow from the one described above, namely it shows that the distance between bubbles changes as $\alpha^{-1/3}$ so that the bubbles in the flow are somewhat ordered, whereas correlation (4) corresponds to a chaotic arrangement of bubbles without a characteristic scale of the distance between them [26]. To elucidate the influence of the type of correlation on the true gas content, a calculation by (5) was also made (see Fig. 8). The maximum gas content is attained in the calculation with correlation (6) and then with (4), and the minimum is attained with (5). From Fig. 8 it is seen that for two-millimeter bubbles up to a certain Reynolds flow number the curve plotted by (4) coincides well with the experimental one. For one-millimeter bubbles the data at small Reynolds numbers lie between the results of the calculations with corrections (4) and (6). At large Reynolds numbers the experiments for both sizes of bubbles gives a systematically understated

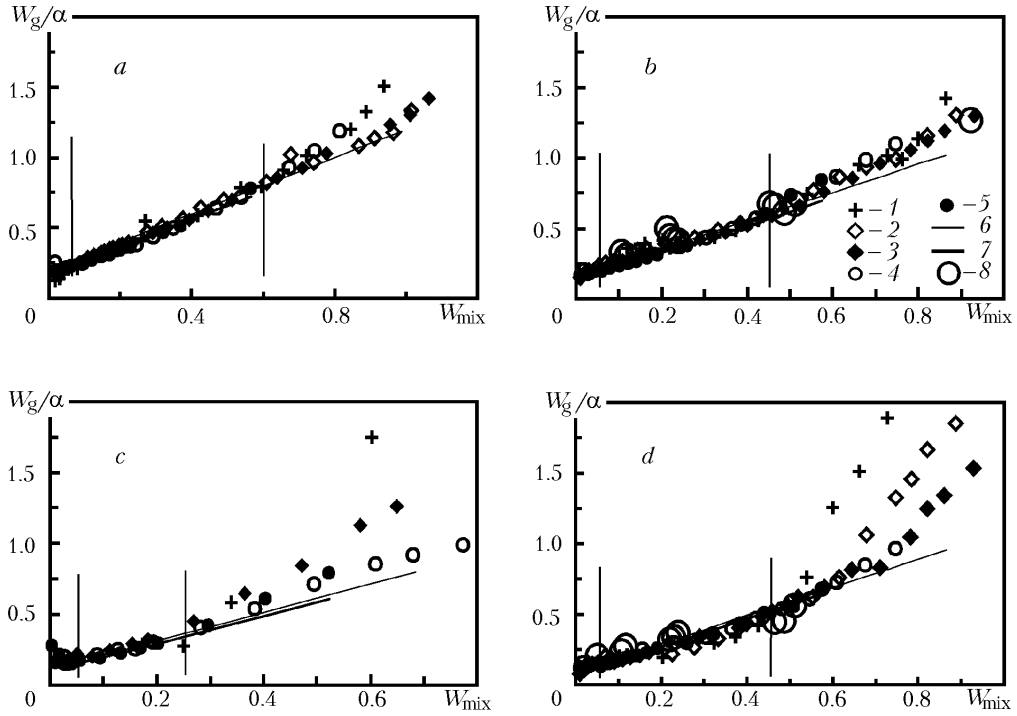

Fig. 9. Zuber and Findley diagrams: a) d_b = 2.2 mm, $\nu = 1.06 \cdot 10^{-6}$ m^2/sec; b) 2.2 and 3.5 $\cdot 10^{-6}$; c) 2.2 and $9.8 \cdot 10^{-6}$; d) 1.2 and $3.5 \cdot 10^{-6}$ [1) β = 0.017; 2) 0.043; 3) 0.0865; 4) 0.130; 5) 0.174; 6) and 7), calculations according to Zuber and Hench [1] with correlation (4) for β = 0.017 and 0.174, respectively; 8) data of [18]. W_g/α, m/sec; W_{mix}, m/sec.

gas content. To verify this deviation, Figure 8 shows additionally the data on the true volume gas content (numbers in circles) plotted by the local gas content profiles [18] obtained under analogous conditions. The local gas content was registered by means of the conduction method and on the assumption of flow symmetry was integrated for the tube cross-section. As mentioned above, asymmetry may be present in the flow. By virtue of contactness of the measuring method, the conduction pickup may give understated values even with the use of ordinary water [13], not to mention viscous process solutions. These two reasons explain the large spread of values of the true gas content estimated with the use of the local gas content profiles. Nevertheless, there is good agreement between the experimental data sets obtained by different methods. Both sets point to a deviation of the experimental gas content from the calculated one for large Reynolds flow numbers. Under laminar and turbulent flow conditions the calculation-experiment relations are analogous. At first there is a good agreement, which is disturbed with increasing Reynolds flow number. The experimental gas content turns out to be systematically lower than the calculated one at Re > 250–500 under laminar flow conditions and at Re > 5000–12,000 under turbulent conditions.

To elucidate the reasons for the deviation, the experimental data are given in the form of Zuber–Findley diagrams (Fig. 9). The results of the calculations according to [1] with the use of (4) for volume gas contents β = 0.017 and 0.174 coincide to an accuracy of 1%. For transient flow conditions, Fig. 9b and d present the data from [18]. Under turbulent, laminar, and transient flow conditions the experimental data up to the limit velocities of the mixture $W_{mix} \approx$ 0.6, 0.45, and 0.25 m/sec, respectively, lie on straight lines practically coinciding with correlation (4). In the Zuber–Findley diagram this corresponds to invariable flow conditions. Interestingly, these limit velocities W_{mix} decrease linearly with increasing viscosity of the process solution. At large velocities of the mixture the experimental data systematically deviate upwards, especially strongly for one-millimeter bubbles. Such behavior in the Zuber–Findley diagram is explained by the change of the flow conditions and is accompanied by a stepwise increase in the parameter C_0. For transient flow conditions the deviation begins at Re $\approx$ 2000 and practically coincides in Reynolds flow number with the onset of the laminar-turbulent transition.

Analysis of the local gas content profiles obtained under analogous experimental conditions [18] shows that in the flow there occurs a change of the gas phase distribution over the tube cross-section. At small Reynolds flow numbers for both bubble sizes used the gas content profiles have a wall-adjacent peak, and at large numbers they change to profiles with a maximum on the tube axis (which is well known from the literature [2–5]). Within the range of low velocities of the mixture the wall-adjacent peak in the gas content profiles is also absent, but the change of flow conditions is practically not noticeable on the Zuber–Findley diagram, since at $W_{mix} \to 0$ the values of W_g/α approach a constant close to the emergence rate of a bubble in a large volume. Therefore, in calculating the Zuber–Findley distribution parameter C_0, as an upper bound of the data used, we took the limit velocity of the mixture corresponding to the beginning of the change of flow conditions, and as a lower bound for all flow conditions and all gas contents we took the mixture velocity W_{mix} = 0.06 m/sec. The data domains used for the calculations are enclosed between the vertical lines in Fig. 9.

The distribution parameter C_0 under turbulent and transient flow conditions for 2/1-mm bubbles is equal, respectively, to 1.09/0.91 and 0.88/0.79, and the drift velocity is 0.142/0.147 and 0.18/0.096 m/sec. Under laminar flow conditions for two-millimeter bubbles C_0 = 0.98 and the drift velocity is 0.124 m/sec. For all tested flow conditions the parameter C_0 for one-millimeter bubbles is smaller than for two-millimeter ones. The distribution parameter is practically independent of the volume gas content.

In [15], an empirical correlation was proposed for the Zuber–Findley distribution parameter for bubbly columns of diameter from 25 to 60 mm:

$$C_0 = (1.2 - 0.2\sqrt{\rho_g/\rho_{liq}})\left(1 - \exp\left(-22\,\frac{d_b}{D}\right)\right). \quad (7)$$

Using this formula for a tube of diameter 14.8 mm leads to overstated values of the parameter C_0 = 1.15 for two-millimeter bubbles and C_0 = 0.99 for one-millimeter ones, and here the influence of viscosity is neglected. At $d_b/D <$ 0.024, when for the given tube $d_b <$ 0.35 mm, $C_0 < 0.5$, and as the bubble diameter decreases to zero, $C_0 \to 0$, which is contrary to reality. In [16], a number of formulas are given for calculating the distribution parameter C_0 in tubes of large diameters (from 0.1 m and more), but for a small-diameter tube all formulas yield overstated values.

CONCLUSIONS

1. Tube-perimeter-averaged friction stresses and its pulsations under laminar, transient, and turbulent flow conditions have been measured. To record the friction amplitude and sign, the electrodiffusion method with dual friction pickups was used. The ratios of average friction to single-phase one for different flow conditions of the mixture are qualitatively similar. At low expenditure velocities of the mixture under all flow conditions negative friction stresses on the wall arise. With further increase in the liquid velocity the friction stress on the wall becomes positive and reaches its maximum, after which the influence of bubbles begins to decrease. An increase in the process solution viscosity and in the average bubble diameter leads to smaller amplitudes of the bubble-induced friction. Such a trend is partly explained by the larger distance of bubbles from the tube wall with increasing solution viscosity and bubble diameter.

2. In friction pulsations on the wall, one can distinguish the regime of reverse flows, the regime of a constant level of pulsations (independent of the Reynolds number), and the regime of pulsations growing with increasing Reynolds number, as in a developed turbulent flow. Pseudoturbulent friction pulsations on the wall under laminar flow conditions differ qualitatively from pulsations under turbulent flow conditions.

3. To estimate the nonuniformity of the friction distribution over the tube cross-section, the friction asymmetry parameter has been introduced. Analysis of the friction stress realizations permits registration of strong-asymmetry flow conditions corresponding to the formation in the induced flow of local bubbly columns.

4. A comparison of the true gas content calculated according to Zuber and Hench [1] to that calculated by correlations (4), (5), and (6) has been made. In so doing, the friction stress on the wall averaged aver the tube perimeter was used. The calculation with correlation (4) well describes the true volume gas content under different flow conditions of the gas-liquid mixture of two-millimeter bubbles with a wall-adjacent peak of the gas content. For one-millimeter bubbles the experimental data of the true gas content are between the calculations with correlations (4)

and (6), which, in particular, points to the possibility of appearance in the flow of a characteristic distance between bubbles and to a structuring of the flow. At large Reynolds flow numbers there is a deviation from the calculation coinciding with the transition from profiles with a wall-adjacent gas content peak to profiles with a gas content maximum on the tube axis, which leads to an increase in the drift velocity of bubbles and a decrease in the true volume gas content. On the Zuber–Findley diagram a change of flow conditions is registered therewith.

This work was supported by the Russian Basic Research Foundation (grant No. 05-01-00687a).

NOTATION

C_0, distribution parameter in the Zuber–Findley theory; D, tube diameter ($D = 2R$), mm; d_b, equivalent bubble diameter, mm; dP/dx, pressure drop per unit length of the tube minus the hydrostatic weight of the pure liquid column, N/m^2; g, gravitational acceleration, m/sec^2; j_{21}, drift velocity of the gas phase; $h(\alpha)$, drag coefficient taking into account the slowing-down of a bubble by surrounding bubbles; K_a, friction asymmetry parameter in (1); R, tube radius, mm; $\mathrm{Re} = W_{liq}D/\nu$, Reynolds number of the tube; $\mathrm{Re}_b = V_\infty d_b/\nu$, Reynolds number of the bubble; T, time, sec; V_∞, emergence rate of a bubble in a free volume, m/sec; W_g and W_{liq}, reduced flow velocities of gas and liquid, respectively, m/sec; $W_{mix} = W_{liq} + W_g$, flow velocity of mixture, m/sec; α, true volume gas content of the flow, dimensionless; $\beta = W_g/(W_g + W_{liq})$, expenditure volume gas content of the flow, m^2/sec; ρ_{liq} and ρ_g, process liquid and gas densities, kg/m^3; τ and τ_0, friction stress on the wall in two-phase and one-phase flows, N/m^2; τ', rms pulsation of the friction stress on the wall, N/m^2. Subscripts: g, gas; liq, liquid; max and min, maximum and minimum values; b, bubble; mix, mixture; a, asymmetry.

REFERENCES

1. N. Zuber and J. Hench, Rept. No. 62GL 100, General Electric Co., Schenectady, New York (1962).
2. M. Kh. Ibragimov, V. P. Bobkov, and N. A. Tychinskii, Investigation of the behavior of the gas phase in a turbulent water–gas mixture flow in channels, *Teplofiz. Vys. Temp.*, **11**, No. 5, 1051–1061 (1973).
3. A. Serizawa, *Fluid-Dynamic Characteristics of Two-Phase Flow*, Ph. D. Thesis, Kyoto University, Japan (1974).
4. Y. Sato, M. Sadatomi, and K. Sekoguchi, Momentum and heat transfer in two-phase bubbly flow, *Int. J. Multiphase Flow*, **7**, 167–177 (1981).
5. S. K. Wang, S. J. Lee, O. C. Jones, and R. T. Lahey, 3D turbulence structure and phase distribution measurements in bubbly two-phase flows, *Int. J. Multiphase Flow*, **13**, 327–343 (1987).
6. N. V. Valukina and O. N. Kashinskii, Investigation of the friction stress on the wall in a monodisperse gas-liquid flow. Characteristic features of the gas-liquid moisture flow at low Reynolds numbers, *Prikl. Mekh. Tekh. Fiz.*, No. 1, 93–98 (1979).
7. J. L. Achard and A. Cartellier, Local characteristics of upward laminar bubbly flows, *PCH*, **6**, No. 5/6, 841–852 (1985).
8. O. N. Kashinsky, L. S. Timkin, and A. Cartellier, Experimental study of "laminar" bubble flow in vertical pipe, *Exp. Fluids*, No. 14, 308–314 (1993).
9. S. P. Antal, R. T. Lahey, and J. E. Flaherty, Analysis of phase distribution in fully developed laminar bubbly two-phase flow, *Int. J. Multiphase Flow*, **17**, 635–652 (1991).
10. Q. Song, R. Luo, X. Y. Yang, and Z. Wang, Phase distribution for upward laminar dilute bubbly flows with non-uniform bubble sizes in a vertical pipe, *Int. J. Multiphase Flow*, **27**, 379–390 (2001).
11. A. Cartellier, O. Kashinsky, and L. Timkin, Experimental characterization of pseudo-turbulence in Poiseuille bubbly flow, in: *Proc. 2nd Int. Conf. on Multiphase Flow*, 3–7 April 1995, Kyoto, Japan (1995), pp. IF1-27–IF1-33.
12. O. N. Kashinskii, R. S. Gorelik, and V. V. Randin, Hydrodynamics of vertical bubbly flows at low liquid phase velocities, in: *Gas-Liquid Flows* [in Russian], Novosibirsk, ITF SO AN SSSR (1990), pp. 44–59.
13. L. S. Timkin, N. Riviere, A. Cartellier, and O. N. Kashinsky, Performance of electrochemical probe for local void fraction measurements in air-water flows, *Rev. Sci. Instrum.*, **74**, No. 8, 3784–3786 (2003).

14. N. Zuber and J. A. Findlay, Average volume concentration of phases in two-phase flow systems, *J. Heat Transfer*, No. 4, 453–467 (1965).
15. T. Hibiki and M. Ishii, Distribution parameter and drift velocity of drift-flux model in bubbly flow, *Int. J. Heat Mass Transfer*, **45**, 707–721 (2002).
16. X. Shen, K. Mishima, and H. Nakamura, Two-phase phase distribution effect on drift–flux parameters in a vertical large diameter pipe, in: *Proc. 3rd Int. Symp. on Two-Phase Flow Modeling and Experimentation*, 22–24 September 2004, Pisa, Italy (2004), CD paper jp26.
17. S. Guet, G. Ooms, R. V. A. Oliemans, and R. F. Mudde, Bubble size effect on low liquid input drift–flux parameters, *Chem. Eng. Sci.*, **59**, 3315–3329 (2004).
18. L. S. Timkin, Measurement of the local slip velocity of bubbles in an upward pseudoturbulent flow, *Teplofiz. Aéromekh.*, **7**, No. 1, 101–114 (2000).
19. V. E. Nakoryakov, A. P. Burdukov, O. N. Kashinskii, and P. I. Geshev, *Electrodiffusion Method for Investigation of Local Characteristics of Turbulent Flows* [in Russian], Novosibirsk, ITF SO AN SSSR (1986).
20. G. B. Wallis, The terminal speed of single drops or bubbles in an infinite medium, *Int. J. Multiphase Flow*, **1**, 491–511 (1974).
21. O. N. Kashinsky and L. S. Timkin, Fluctuating wall shear stress in upward pseudo-turbulent bubbly flow, in: G. P. Celata, P. D. Marco, and R. K. Shah (Eds.), in: *Proc. Second Int. Symp. "Two-Phase Flow Modeling and Experimentation 1999,"* 23–26 May 1999, Rome, Italy (1999), Vol. 2, pp. 1117–1121.
22. J. Laufer, *The Structure of Turbulence in Fully Developed Pipe Flow*, NACA, Rep. 1174 (1954), pp. 1–18.
23. L. S. Timkin, R. S. Gorelik, and P. D. Lobanov, Emergence of a single bubble in upward laminar flow: slip velocity and wall friction, *Inzh.-Fiz. Zh.*, **78**, No. 4, 129–135 (2005).
24. J. B. Joshi, V. S. Vitankar, A. A. Kulkarni, M. T. Dhotre, and K. Ekambara, Coherent flow structures in bubble column reactors, *Chem. Eng. Sci.*, **57**, 3157–3183 (2002).
25. C. Garnier, M. Lance, and J. L. Marie, Measurement of local flow characteristics in buoyancy-driven bubbly flow at high void fraction, *Exp. Thermal Fluid Sci.*, **26**, 811–815 (2002).
26. R. H. Davis and A. Acrivos, Sedimentation of noncolloidal particles at low Reynolds numbers, *Ann. Rev. Fluid Mech.*, **17**, 91–118 (1985).